Boletín de la Sociedad Española de Cerámica y Vidrio
Vol 53, 3, 121-132, Mayo-Junio 2014 ISSN 0366-3175. eISSN 2173-0431.
doi: 10.3989/cyv.162014

BOLETIN DE LA SOCIEDAD ESPAÑOLA DE
Cerámica y Vidrio
A R T I C U L O

Solid state reaction synthesis of $Ba_{0.75}Sr_{0.25}AlSi_2O_8$ - Al_2O_3 ceramic composites from mechanically activated precursor mixtures

M. V. RAMOS-RAMÍREZ, J. LÓPEZ-CUEVAS*, J. L. RODRÍGUEZ-GALICIA AND J. C. RENDÓN-ANGELES

CINVESTAV-IPN, Unidad Saltillo, Calle Industria Metalúrgica, No. 1062, Parque Industrial Saltillo - Ramos Arizpe, Ramos Arizpe, Coahuila, México, CP 25900
*Corresponding author. Tel. +52 844 4389600; fax: +52 844 4389610. E-mail address: jorge.lopez@cinvestav.edu.mx (J. López-Cuevas)

Ceramic composites with $Ba_{0.75}Sr_{0.25}AlSi_2O_8$ (SBAS)/Al_2O_3 mass ratios of: 1) 90/10, 2) 70/30, and 3) 50/50, were *in situ* synthesized at 900-1500 °C/5 h from mixtures of fly ash, $BaCO_3$, $SrCO_3$ and Al_2O_3. The green mixtures were mechanically activated for 0, 4 and 8 h in an attrition mill. As a result, the solid state reactions were faster and occurred at lower temperatures. Only the SBAS and Al_2O_3 phases were obtained at 1300-1500°C, with the SBAS present in composition 1 achieving full conversion from its hexagonal (Hexacelsian) into its monoclinic (Celsian) form, with or without milling. The higher nominal SBAS content of composition 1 facilitated in it the mentioned conversion, in comparison with the other two studied compositions, which required to be mechanically activated for times that increased with increasing Al_2O_3 content, in order to attain in them similarly high Hexacelsian to Celsian conversions. The mechanical properties of the synthesized materials increased with increasing milling time, sintering temperature and Al_2O_3 content. Thus, the best mechanical properties were obtained for composition 3 milled for 8 h and sintered at 1500 °C.

Keywords: Mechanical Activation, Ceramic Composites, Celsian, Coal Fly Ash.

Síntesis por reacción en estado sólido de compósitos cerámicos $Ba_{0.75}Sr_{0.25}AlSi_2O_8$ - Al_2O_3 a partir de mezclas precursoras activadas mecánicamente

Compósitos cerámicos con relaciones $Ba_{0.75}Sr_{0.25}AlSi_2O_8$ (SBAS)/Al_2O_3 en masa de: 1) 90/10, 2) 70/30, y 3) 50/50, fueron sintetizados *in situ* a 900-1500 °C/5 h usando mezclas de cenizas volantes, $BaCO_3$, $SrCO_3$ y Al_2O_3. Las mezclas en verde fueron activadas mecánicamente por 0, 4 y 8 h en un molino de atrición. Como resultado, las reacciones en el estado sólido fueron más rápidas y ocurrieron a menores temperaturas. A 1300-1500°C sólo se obtuvo las fases SBAS y Al_2O_3, con el SBAS presente en la composición 1 transformado completamente de su forma hexagonal (Hexacelsiana) a la monoclínica (Celsiana), con o sin molienda. El mayor contenido nominal de SBAS en esa composición facilitó dicha conversión, en comparación con las otras dos composiciones estudiadas, las cuales requirieron ser activadas mecánicamente por tiempos que se incrementaron con el incremento en su contenido de Al_2O_3, para que pudiesen alcanzar conversiones Hexacelsiana a Celsiana similarmente altas. Las propiedades mecánicas de los materiales sintetizados se incrementaron con el incremento en el tiempo de molienda, en la temperatura de sinterización y en el contenido de Al_2O_3. De esta manera, las mejores propiedades mecánicas correspondieron a la composición 3 molida por 8 h y sinterizada a 1500 °C.

Palabras clave: Activación Mecánica, Compósitos Cerámicos, Celsiana, Cenizas Volantes.

1. INTRODUCTION

The $Ba_{1-x}Sr_xAl_2Si_2O_8$ (SBAS) solid solutions are attractive as matrixes for ceramic composites for structural applications at high temperatures. The SBAS solid solutions can be potentially useful for environmental barrier coatings (EBCs) such as those employed for Si-based (SiC, Si_3N_4) ceramic components in the hot section of advanced gas turbine engines (1), as well as for X-ray radiation-shielding applications (2) and for the fabrication of missile nose cones (radomes) (3), among other applications. These materials can be obtained by partial substitution of BaO by SrO in $BaAl_2Si_2O_8$ (BAS) (4,5), or alternatively from mixtures of BAS with $SrAl_2Si_2O_8$ (SAS) (6). The formation of SBAS obeys Vegard's law and it can take place over the entire concentration range ($0 \le x \le 1$) (5,7). Both BAS and SBAS are denominated either as Celsian (or Monocelsian) when their crystalline structure is monoclinic, or as Hexacelsian when they have a hexagonal lattice structure. The monoclinic phase is of particular interest due to its high refractoriness, low coefficient of thermal expansion (CTE), good resistance to oxidation and to slag attack, and good thermal shock resistance (4). However, the hexagonal phase is frequently formed first, tending to remain in a metastable state at low temperatures. This phase is undesirable due to its relatively high CTE and because it might transform into an orthorhombic polymorphic form during cooling of the material, which causes differential volume changes in the latter, leading to the generation of microcracks that affect negatively its final mechanical properties (8). Once Hexacelsian has been formed, its conversion into Celsian

tends to be difficult and sluggish, especially in the case of BAS, since the presence of SrO facilitates this conversion in SBAS. D. Long-González et al. (5) recommended employing SBAS compositions containing SrO in the range of $0.25 \leq x \leq 0.375$, in order to obtain Celsian with optimum properties.

The stabilization of Celsian in BAS, and presumably also in SBAS, can be achieved by doping the material with mineralizing agents such as Li_2O, NaF, CaO, TiO_2, MgO, SrF_2, BeO and Cr_2O_3 (9,10). The efficiency of this method depends on the nature and amount of the added mineralizer. The stabilization of Celsian also depends on the nature of the employed initial raw materials (11-15), as well as on the conditions used for the synthesis of BAS (5,16,17). For instance, the formation of Hexacelsian is usually favored by a diminution in the particle size of the precursor materials. It is known (17) that while Celsian tends to nucleate in the bulk, Hexacelsian tends to do it at the surface of the precursor particles. Mechanical activation of the precursor mixture is a well-known way to promote the surface nucleation of Hexacelsian. It has been hypothesized that the very fine particles with fresh surfaces created by the milling process provide the necessary conditions for the surface nucleation of Hexacelsian.

On the other hand, it is known that Al_2O_3 and BAS, as well as Al_2O_3 and SAS, are chemically compatible (i.e., they are chemically stable in the presence of each other) at subsolidus temperatures, since a tie line exists between Al_2O_3 and BAS (18,19), as well as between Al_2O_3 and SAS (19-21), in the corresponding ternary phase equilibrium diagrams. In consequence, in the solid state, both BAS and SAS are able to coexist at equilibrium with Al_2O_3 over a broad temperature range. Taking this into account, solid Al_2O_3 is also very likely to be chemically compatible with solid SBAS over a broad temperature range, but further research work is needed in order to verify this experimentally. Except for some preliminary results previously reported by us (22), no additional information was found in the published literature regarding studies involving the synthesis and characterization of SBAS-Al_2O_3 ceramic composites.

SBAS-Al_2O_3 composites in which SBAS was present as Celsian were of particular interest for us. Driven by the lack of published information on this system, as well as by their potential structural applications at high temperatures, we set out to study the *in situ* synthesis of SBAS - Al_2O_3 composites, with SBAS having a composition of $Ba_{0.75}Sr_{0.25}Al_2Si_2O_8$, by a solid state reaction of precursor mixtures composed of fly ash (FA, byproduct of a coal-burning power plant), $BaCO_3$, $SrCO_3$, and Al_2O_3, with the precursor mixtures subjected to prior mechanical activation. Typically, FA is composed mainly by SiO_2-rich glassy phase plus α-quartz, mullite ($Al_6Si_2O_{13}$), iron oxides (FeO, Fe_3O_4, Fe_2O_3), alkaline and alkaline-earth oxides, as well as some heavy metal and transition metal oxides (23). It is worth mentioning that only in some previous instances FA has been used as a raw material for the synthesis of either BAS or SBAS (5,24-26), despite the fact that it has been observed (5,24) that some of the FA impurities (Na_2O, CaO, TiO_2 and MgO) could act as mineralizers that enhance the Hexacelsian to Celsian conversion in these materials, with or without prior mechanical activation of the corresponding precursor mixtures. C.M. López-Badillo et al. (24) synthesized BAS by a solid state reaction process, using FA, $BaCO_3$ and Al_2O_3 as raw materials. The precursor mixture was mechanically activated in an attrition mill for up to 12 h and then sintered in the temperature range of 900-1300 °C. It was found that the reaction rate, the apparent density and the mechanical properties of the synthesized materials increased with increasing milling time and sintering temperature. It was concluded that the mineralizing effect caused by the mentioned FA impurities aided to overcome the stabilizing effect of mechanical activation on the Hexacelsian phase, resulting in Hexacelsian to Celsian conversions higher than those previously reported by S. Bosković et al. (17) for BAS materials synthesized from mechanically-activated reagent grade raw materials.

The main objective of this work was to study the dependence of the phase composition, and physical and mechanical properties of the synthesized composite materials, on their SBAS/Al_2O_3 weight ratio as well as on the conditions employed for the prior mechanical activation given to the precursor mixtures and temperature used for their posterior reactive sintering.

2. EXPERIMENTAL PROCEDURE

2.1. Preparation of the precursor mixtures

Three $Ba_{0.75}Sr_{0.25}AlSi_2O_8$ (SBAS) - Al_2O_3 composite compositions, with SBAS/Al_2O_3 mass ratios of: 1) 90/10, 2) 70/30, and 3) 50/50, hereinafter referred to as compositions 1, 2 and 3, respectively, were *in situ* synthesized by reactive sintering, from precursor mixtures prepared using the following raw materials: Coal fly ash (FA, silicoaluminous byproduct of a Mexican coal-burning power plant); Al_2O_3 (with purity of 99.99 wt. % and particle size <1 μm, SASOL HPA-0.5, USA); $BaCO_3$ (with purity of 99.43 wt. % and particle size of ~3 μm, Alkem, México), and $SrCO_3$ (with purity of 97.83 wt. % and particle size of ~4 μm, Solvay, México).

Except for the FA, all the other raw materials were used as received. After milling for 1 h in a ball mill, the FA was subjected to a manual wet magnetic separation process, using for this a neodymium magnet with an intensity of 12,300 Gauss, which reduced in ~45 wt. % the original content of iron oxides of this material. This was carried out in order to minimize the formation of iron-rich low-melting point secondary phases during reactive sintering of the materials. The chemical composition of the conditioned FA, as determined by semiquantitative short wavelength dispersive X-Ray Fluorescence (XRF) spectroscopy using a S4 PIONEER BRUKER apparatus, was (wt. %): 64.48 % SiO_2, 27.28 % Al_2O_3, 2.33 % Fe_2O_3, 2.44 % CaO, 0.64 % MgO, 0.62 % TiO_2, 0.28 % K_2O, 0.18 % Na_2O and 0.19 % of other oxides (ZrO_2, MnO_2, SrO, PbO and P_2O_5). Thermogravimetry (TGA) revealed that this material contained also 1.73 % of free C. All TGA analyses were carried out up to a maximum temperature of 1400°C, employing a PERKIN ELMER Pyris Diamond TG/DTA apparatus, platinum crucibles and heating rate of 10°C/min in still ambient air. The particle size of the conditioned FA was ~30 μm. All particle size determinations were carried out by laser diffraction using a Coulter LS-100 apparatus. X-Ray Diffraction (XRD) indicated that the conditioned FA was mainly composed by α-quartz and Mullite ($Al_6Si_2O_{13}$) crystalline phases. All the XRD studies were carried out using a Philips X-PERT 3040 equipment and Cuk_α radiation,

with a scanning speed of 0.03° /s, in the 2θ interval from 2° to 60°. Dissolution of the conditioned FA with HF acid (5) allowed us to estimate that it also contained ~70 wt. % of a silicoaluminous glassy phase. It is worth mentioning that the presence of this glassy phase in the employed FA could aid the sintering process of the ceramic composites by the generation of a small amount of a transient liquid. On the other hand, since the used FA had a content of SiO_2 + Al_2O_3 + Fe_2O_3 higher than 70 wt. %, it was determined that it belonged to the F type, according to the ASTM C618 standard (27). In the case of the other raw materials employed, the corresponding phase composition and low level of impurities were only qualitatively verified by XRD.

Only the conditioned FA was used for the preparation of the precursor mixtures required for the synthesis of the studied SBAS-Al_2O_3 composite compositions, according to the stoichiometric proportions of the employed raw materials shown in Table I.

TABLE I. STOICHIOMETRIC COMPOSITIONS (WT. %) OF THE PRECURSOR MIXTURES USED FOR THE SYNTHESIS OF THE STUDIED SBAS-Al_2O_3 COMPOSITES.

Composition	FA	Al_2O_3	$BaCO_3$	$SrCO_3$
1	39.6	20.80	31.52	8.12
2	38.80	38.40	24.52	6.40
3	22.00	56.00	17.60	4.40

It is worth mentioning that the employment of FA provided by other coal-burning power plants, which was generated using coal with different mineralogical characteristics, would result in a variation in the chemical and phase composition of this raw material with respect to that used in the present work. In order to try to counteract the effect of the mention variation on the chemical and phase composition of the final ceramic products, as well as on the properties of the latter, we offer the following recommendations to the potential readers of this paper who could be interested in reproducing any part of the experimental work reported in it: 1) stick to the use of F type FA, which contains less than 20 wt. % of CaO; small variations in the content of the latter oxide could be acceptable, since the levels at which it is usually present in the F type FA facilitates the Hexacelsian to Celsian conversion (5), 2) subject the FA to a magnetic separation process until it achieves a level of iron oxides similar to that achieved in the FA employed by us, and 3) determine accurately the chemical composition of the conditioned FA, since it would be the basis for the calculation of the relative proportions of $BaCO_3$, $SrCO_3$ and Al_2O_3 required for the synthesis of ceramic materials with the desired chemical composition.

2.2. Mechanical activation of the precursor mixtures

The stoichiometric precursor mixtures were homogenized and subjected to a high energy milling in a Teflon-lined closed chamber laboratory attrition mill operated at 1700 rpm, for times of 0, 4 and 8h, employing 8 mol. % MgO-partially-stabilized ZrO_2 balls as milling media, with a balls to load mass ratio of 5:1, and using ethylic alcohol as dispersion medium. All precursor mixtures, with or without mechanical activation, were analyzed by XRD, TGA and particle size. It was found that after 8h of milling, the mean particle size of the precursor mixtures decreased from 21.6 to 6.3μm for composition 1, from 17.7 to 3.9μm for composition 2, and from 13.7 to 2.8μm for composition 3.

2.3. Reactive sintering

Prior to the solid state reaction process, a portion of all precursor mixtures were uniaxially pressed into 1.5g-cylinders with dimensions of 1.2 cm (diameter) x 0.5 cm (height), applying a load of 4 Ton. The rest of the powders of all compositions were uniaxially pressed into prismatic bars with a length of 7 cm, a width of 3 cm, and a height of 5 cm, applying a load of 7 Ton. In both cases a CARVER INC 4350 press was used. Then, the cylinders and the prismatic bars were sintered using a Thermolyne 46120-CM-33 high temperature electric furnace, at a temperature range of 900-1500°C, in steps of 200°C, with heating and cooling rates of 2 and 5°C/min, respectively, with a holding time at temperature of 5 h in the case of the cylinders, and of 8 h for the prismatic bars. In all cases, the furnace was turned off after completion of the reactive sintering treatment, allowing the samples to cool down to room temperature in a natural way inside the furnace.

2.4. Phase composition of the sintered materials

All sintered materials were analyzed by XRD and SEM/EDS, using for the latter technique a JEOL-6300 SEM apparatus, with an acceleration voltage of 15 kV and working distance of 8 mm. For microstructural analysis, the sintered cylinders were cross-sectioned by using a diamond saw. This was followed by mounting one half of each sample in cold-cure epoxy resin and then by grinding its cut surface using SiC papers with successive grit sizes from 80 grit to 2400 grit. The ground surface was then polished to a mirror finish using diamond particles with successive sizes of 3, 1 and ¼ μm, and then graphite-coated using a JEOL JEE-400 vacuum evaporator. For the XRD analysis, the remnant halves of the sintered cylinders were crushed using a synthetic sapphire mortar and pestle, until a particle size of 25-75 μm was achieved. The JCPDS cards no. 381451, 881048 and 751865, were used for the identification of the XRD reflections of Celsian, Hexacelsian, and Al_2O_3 phases, respectively, in the sintered materials.

XRD was also used in order to quantify the phases detected in the sintered samples, with the aid of the XPowder 2004.04 software, which uses non-linear least squares methods and weighting achieved by means of the normalized RIR method described by F.H. Chung (28). The Hexacelsian to Celsian conversion fraction (f, %) was calculated using the weight percentages determined by XRD for both phases, together with the following expression:

$$f = \left(\frac{\%Celsian}{\%Celsian + \%Hexacelsian} \right) x100 \quad (1)$$

2.5. Evaluation of the relative density of the sintered materials

The relative density (ρ_r, g/cm^3) of the sintered materials was determined by using equation 2. The real density (ρ_R, g/cm^3) of the powders that were obtained after crushing one

half of each one of the sintered cylinders was determined by picnometry at room temperature (~25 °C), using equation 3. The theoretical density (ρ_T, g/cm^3) of the nominal composite compositions was calculated using the Rule of Mixtures (29), employing a density of 3.314 g/cm^3 for monoclinic $Ba_{0.75}Sr_{0.25}Al_2Si_2O_8$ taken from the JCPDS card no. 381451, as well as a density of 3.97 g/cm^3 reported by the supplier of the employed Al_2O_3.

$$\rho_r = \frac{\rho_R}{\rho_T} \tag{2}$$

$$\rho_R = \left(\frac{(m_1 - m)*(\rho_t - \rho_a)}{(m_3 + m_1 - m - m_2)} \right) + \rho_a \tag{3}$$

In these equations: ρ_t = density of the liquid (Toluene) used to carry out the picnometric determination, and ρ_a = density of air (0.001 g/cm^3), both of them at the temperature of the assay; m = weight of the dry picnometer (g); m_1 = weight of the dry picnometer + weight of the dry sample (g); m_2 = weight of the dry picnometer + weight of the dry sample + weight of the liquid (Toluene) (g), and m_3 = weight of the dry picnometer + weight of the liquid (Toluene) (g).

2.6. Evaluation of mechanical properties of the sintered materials

The Young's modulus of the sintered prismatic bars was evaluated by using two alternative techniques: a) Pulso-echo ultrasonic inspection technique, and b) Four-point flexural strength test. A Panametrics-NDT™ EPOCH 4 apparatus was used for the pulse-echo ultrasonic inspection technique. In this case, the Young's modulus was determined by measuring the speed of sound propagating through the materials as well as with the aid of equation 4 (30):

$$E(U) = 0.757 \rho V_L^2 \tag{4}$$

where E(U) = Young's modulus (GPa) determined by the pulse-echo ultrasonic technique, ρ = apparent density of the material (Kg/m^3) determined by the Archimedes' principle in distilled water at room temperature, and V_L = longitudinal speed of the ultrasonic wave propagating through the material (m/s).

Once E(U) was obtained, the sintered prismatic bars were cut by using a Struers Accutom-5 cutting machine fitted with a diamond disc, with a cutting speed of 0.015 mm/s, and employing water as lubricant. This was carried out in order to obtain specimens with dimensions specified by the ASTM C1161-02 standard (31) for the evaluation of the modulus of rupture (MOR), as well as specimens for the evaluation of the fracture toughness (K_{IC}), according to the ASTM STP601 standard (32). In both cases, four-point flexural strength tests were employed, using a MTS 810 mechanical testing machine with a 10-ton load capacity, employing a rate of load application (crosshead speed) of 0.05 mm/s until fracture of the specimens, as well as distances between support points of 40 and 20 mm for the inferior and superior sample faces, respectively. Prior to mechanical testing, in order to avoid surface defects, all the cut surfaces of the samples were ground and polished following the procedure mentioned before. The Young's modulus of the materials was determined from the slope of the elastic region of the corresponding stress-strain curves, employing equation 5 (33):

$$E(MT) = \frac{11PL^3}{64bd^3D} \tag{5}$$

where E(MT) = Young's modulus (GPa) determined by four-point flexural strength test, P = applied load (N), L = distance (mm) between support points, b = sample width (mm), d = sample height (mm), and D = sample deflection (mm).

The MOR of the sintered materials was alternatively determined from the slope of the elastic region of the stress-strain curves, employing equation 6 (31):

$$MOR = \sigma = \frac{3PL}{4bd^2} \tag{6}$$

where σ = maximum fracture strength (Pa), P = applied load (N), L = distance between support points (mm), b = sample width (mm), and d = sample height (mm).

The K_{IC} values were determined by employing notched specimens and equation 7 (34):

$$K_{Ic} = \sigma_f Y \sqrt{a}$$
$$Y = 1.99 - 2.47\left(\frac{a}{h}\right) + 12.97\left(\frac{a}{h}\right)^2 - 23.17\left(\frac{a}{h}\right)^3 + 24.8\left(\frac{a}{h}\right)^4 \tag{7}$$

where K_{IC} = critical stress intensity factor or fracture toughness (MPa·m$^{1/2}$), Y = dimensionless parameter which depends on the size and geometry of the sample and of the sample's notch, as well as on the load application mode, a = length of the sample's notch (m), h = height of the sample's notch (m), and σ_f = maximum stress applied for crack propagation (N).

Lastly, the Vickers microhardness (HV) of the polished halves of the sintered cylinders was determined by using a Wilson Tukon 300-FM apparatus, applying a load of 5 Kgf for 5 s and employing a square-based diamond pyramid indenter with an apical angle of 136°. The measurements were made in ten randomly selected points per each sample; the mean values of these measurements are reported in this work. The indentations were measured by using an Olympus VANOX optical microscope coupled to an image analysis system fitted with the Image-Pro Plus software. The Vickers microhardness was determined based on the ASTM E384-99 standard, using equation 8 (35):

$$HV = \frac{1.85P}{a^2} \tag{8}$$

where HV = Vickers microhardness (Kg/mm^2), P = applied load (Kgf), and a = diagonal length of the indentation (mm).

Bol. Soc. Esp. Ceram. Vidr. Vol 53. 3, 121-132, Mayo-Junio 2014. ISSN 0366-3175. eISSN 2173-0431. doi: 10.3989/cyv.162014

3. RESULTS AND DISCUSSION

3.1. Thermal analysis of the precursor mixtures

The TGA curves of Figure 1 show that all samples started losing weight since the very beginning of the heating stage, which was probably due to the release of water adsorbed on the surface of the particles. In all cases, with increasing milling time the rate of weight loss increased. At the same time, the temperature at which the main weight loss stage ended (T_f) was shifted toward lower values and the total weight loss decreased. The latter phenomenon was likely due to a partial decomposition of the $BaCO_3$ and $SrCO_3$ carbonates during the milling stage, whose extension was proportional to the duration of this operation. All these effects were more pronounced with increasing carbonate content in the precursor mixtures, which suggests that $BaCO_3$ and $SrCO_3$ were the most affected by mechanical activation, in comparison with the other components of the precursor mixtures. It is known that mechanical activation of both carbonates decreases both the temperature and the activation energy required for their thermal decomposition, increasing at the same time their reactivity toward other compounds mixed with them (36). After 8h of milling, T_f was shifted from ~1033°C to ~883°C (ΔT = 150°C) for composition 1, with a corresponding total weight loss decreasing from 11.1 % to 9.1 % (Δm = 2 %). For composition 2, T_f was shifted from ~1020°C to ~920°C (ΔT = 100°C), with a total weight loss decreasing from 9.4 % to 7.6 % (Δm = 1.8 %). Lastly, for composition 3, T_f was shifted from ~1013°C to ~923°C (ΔT = 90°C), with a total weight loss of ~6.4 % (Δm ~ 0 %). Since the observed weight losses were mostly caused by the release of CO_2 associated with the occurrence of the solid state reactions, the obtained results mean that these reactions took place at lower temperatures, and at faster rates, in the mechanically activated precursor mixtures, in comparison with the non-milled materials. This could be attributed to the high degree of disorder introduced into the crystalline structure of $BaCO_3$ and $SrCO_3$ by the high-energy milling, as well as to the high degree of homogeneity and small particle size achieved in the precursor mixtures as a result of the milling process.

Despite the fact that $BaCO_3$ and $SrCO_3$ that are present in the precursor mixtures do not decompose at the same temperatures at which they usually do it individually and separately, both carbonates can be considered as adequate references to justify the TGA results obtained in the present work, especially taking into account the fact that the main weight losses suffered by the materials were caused by the release of CO_2 from both carbonates participating in the solid state reactions, as already mentioned.

3.2. Phase composition of the green and sintered samples

The XRD patterns obtained for all the green samples (not shown), with or without mechanical activation, revealed only the presence in them of the original raw materials ($BaCO_3$, $SrCO_3$, Al_2O_3, and α-quartz contained in the FA). The partial decomposition of both carbonates likely occurring during the milling process, as suggested by the TGA analyses, was not detected by XRD, probably due to its small extent. It was observed that the reflections of all detected crystalline phases tended to become broader and less intense with increasing milling time. This was attributed to a small loss in their crystallinity caused by mechanical activation, implying that the milled green materials underwent a partial amorphization. However, the characteristic "hump" associated with the

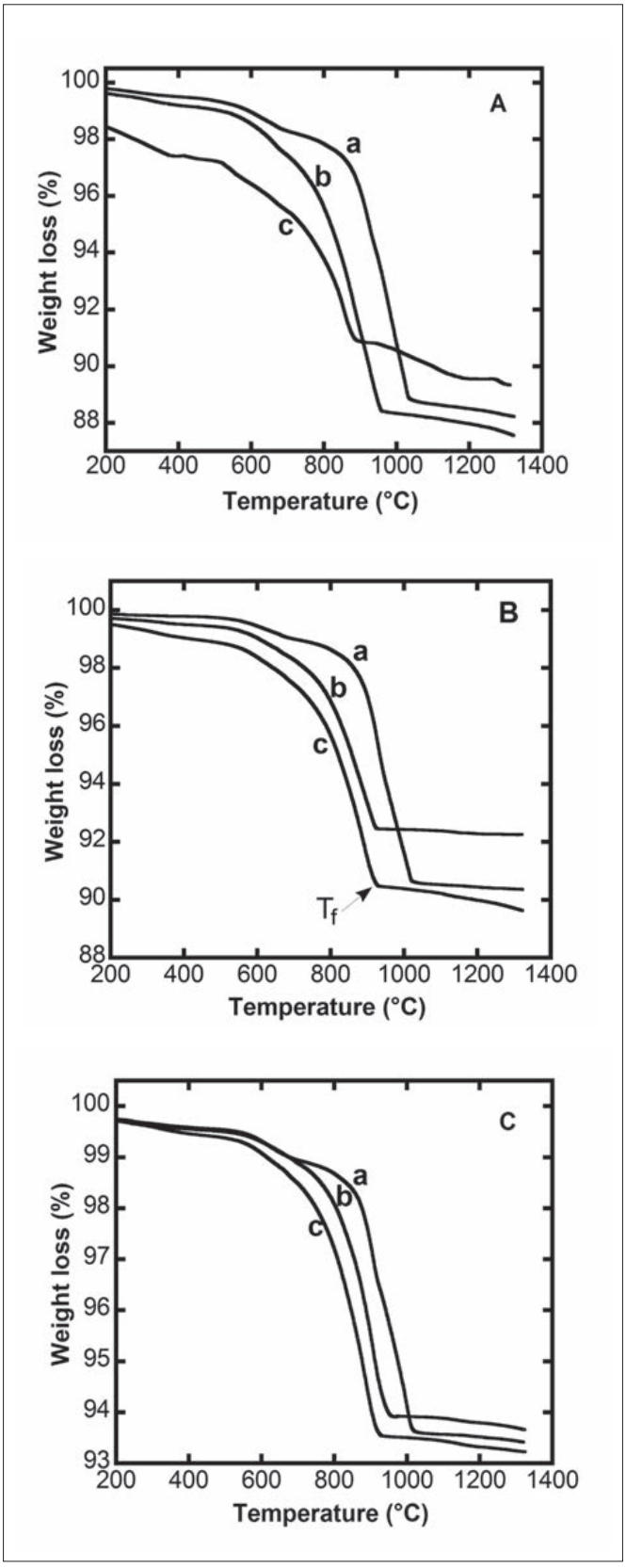

Figure 1. TGA curves obtained for precursor mixtures of compositions 1 (A), 2 (B) and 3 (C), milled for: a) 0 h, b) 4 h and c) 8 h. T_f = Temperature at which the main weight loss stage ends in the materials.

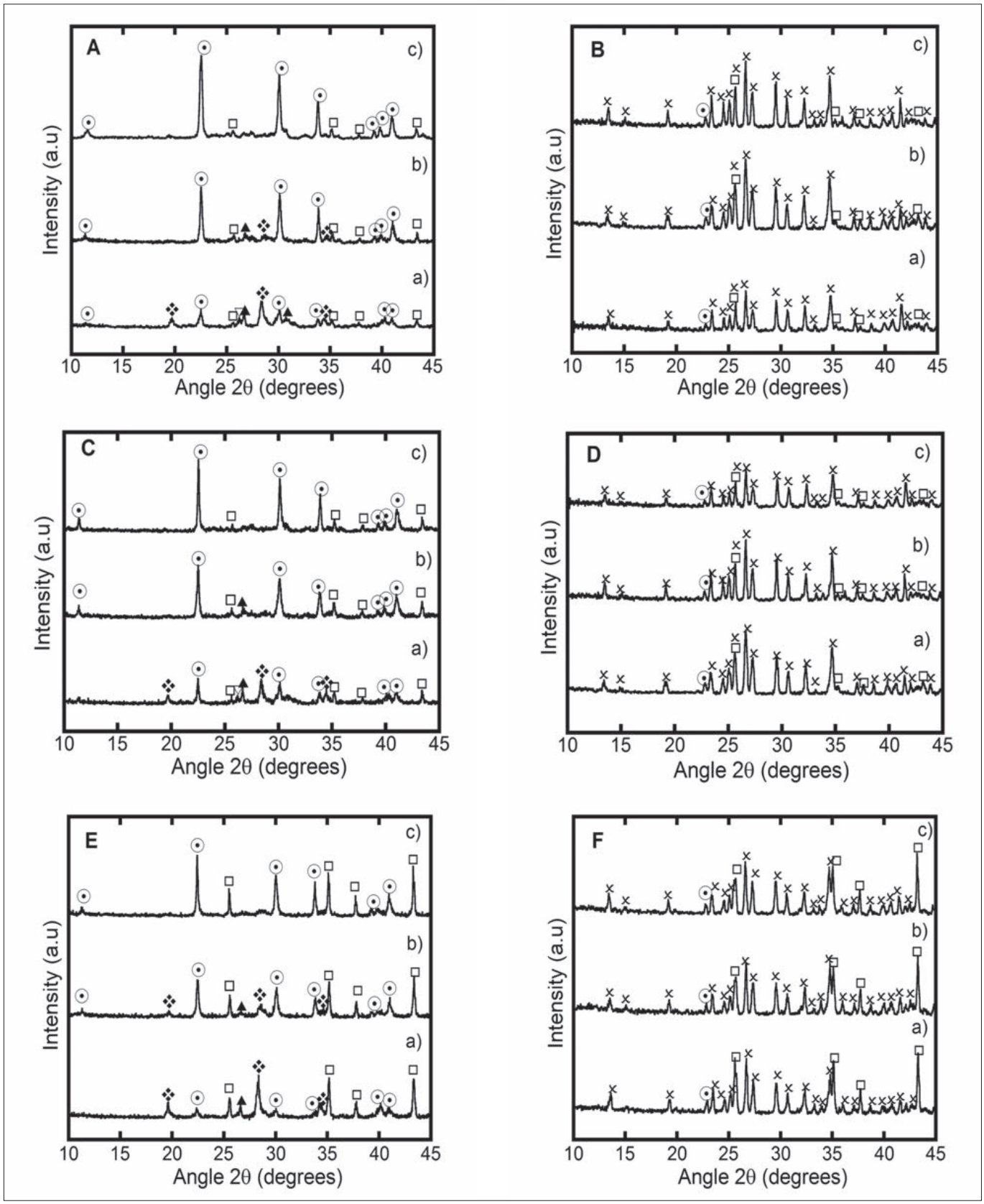

Figure 2. XRD patterns obtained for compositions 1 (A and B), 2 (C and D) and 3 (E and F), milled for: a) 0 h, b) 4 h, and c) 8 h, and then sintered at either 900 °C (A, C and E) or 1500 °C (B, D and F), where: ▲$BaSiO_3$, ▽Ba_2SiO_4, ❖$BaAl_2O_4$, □Al_2O_3, ×Celsian, and ⊙Hexacelsian.

appearance of amorphous phases in the mechanically-activated materials were not clearly detected in the corresponding XRD patterns.

Figure 2 shows the XRD patterns obtained for the samples sintered at either 900 ºC or 1500 ºC, with or without mechanical activation. As it can be seen in the XRD patterns A, C and E,

Bol. Soc. Esp. Ceram. Vidr. Vol 53. 3, 121-132, Mayo-Junio 2014. ISSN 0366-3175. eISSN 2173-0431. doi: 10.3989/cyv.162014

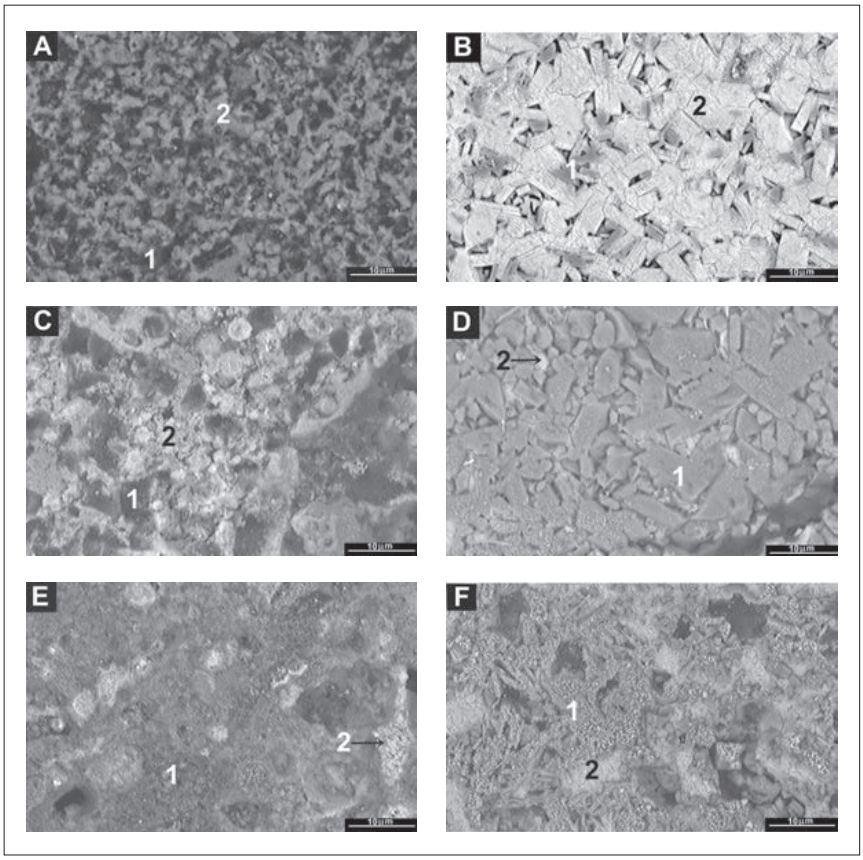

Figure 3. SEM micrographs taken in the Backscattered Electron Imaging (BEI) mode for samples without mechanical activation of compositions 1 (A and B), 2 (C and D) and 3 (E and F), and then sintered at either 900 ºC (A, C and E) or 1500 ºC (B, D and F). Key: 1) Al_2O_3 and 2) SBAS phases.

all of which correspond to samples sintered at 900 °C, at this temperature Hexacelsian was the predominant phase in all compositions, independently of milling time. Minor amounts of $BaSiO_3$, $BaAl_2O_4$, Al_2O_3 and Ba_2SiO_4 were also detected in these samples; the latter phase was found only in non-milled composition 1. It was observed that $BaSiO_3$ disappeared in all compositions milled for 8 h, while $BaAl_2O_4$ disappeared in compositions 1 and 2 milled for 4 h and in composition 3 milled for 8 h. This indicates that at 900 °C the persistence of the $BaAl_2O_4$ phase increased with increasing Al_2O_3 content in the precursor mixture, and thus, under these conditions increasingly longer milling times were required in order to achieve full elimination of the mentioned phase. This is consistent with the results reported by K.-T. Lee and P.B. Aswath (16), who mentioned that $BaAl_2O_4$ is difficult to eliminate once it is formed during the synthesis of BAS, due to its pretty low reaction rate with SiO_2 to form Hexacelsian.

In contrast, only SBAS (Hexacelsian and Celsian) and Al_2O_3 phases were found in the materials of all compositions sintered at either 1300°C or 1500°C. At both sintering temperatures, Celsian was the predominant phase in all samples, as it can be seen in Figure 2 for the case of the composites sintered at 1500 °C (XRD patterns B, D and E).

3.3. Microstructural evolution in the sintered samples

For all compositions and milling times employed, the materials sintered at 900°C showed a poorly-defined microstructure, which was more accentuated in the case of the non-mechanically activated materials, as it can be seen in micrographs A, C and E of Figures 3 and 4. This was probably due to unfinished solid state reactions combined with a poor densification of the samples achieved at such low sintering temperature. It was observed that the main effect of mechanical activation at this temperature was a somewhat increased degree of consolidation of the samples with increasing milling time.

At 1500°C a well-defined microstructure constituted by two phases was observed, as it can be clearly seen in micrographs B, D and F of Figure 4. These phases were: 1) Dark grey platelet and blocky-shaped Al_2O_3 grains, and 2) light-colored SBAS (Hexacelsian + Celsian) polyhedral grains. These phases were identified in the micrographs with the aid of the corresponding EDS spectra (Figure 5). The grain size of both phases ranged from ~5 to ~10 μm, with the smallest grains found in composition 3. While in the case of compositions 1 and 2 the Al_2O_3 grains were heterogeneously dispersed in the SBAS matrix, in composition 3 both phases were homogeneously distributed throughout the microstructure, which is likely associated with the smallest grain size achieved by this composition. In all cases, a large number of intergranular microcracks was formed in the SBAS matrix during cooling after sintering of the materials, probably due to a mismatch existing in the CTE values of Hexacelsian, Celsian and Al_2O_3 phases. For instance, the CTE value reported in the literature for Celsian is $2.3x10^{-6}$ $°C^{-1}$ (16), while that for alumina is $8.4x10^{-6}$

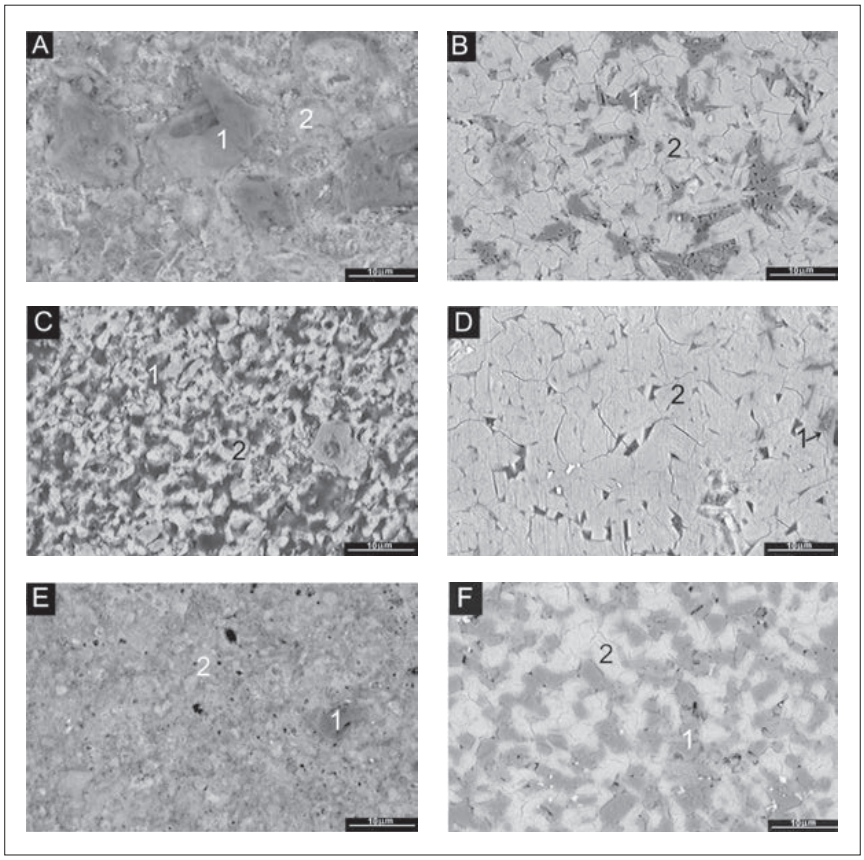

Figure 4. SEM micrographs taken in the Backscattered Electron Imaging (BEI) mode for samples milled for 8 h of compositions 1 (A and B), 2 (C and D) and 3 (E and F), and then sintered at either 900 ºC (A, C and E) or 1500 ºC (B, D and F). Key: 1) Al_2O_3 and 2) SBAS phases.

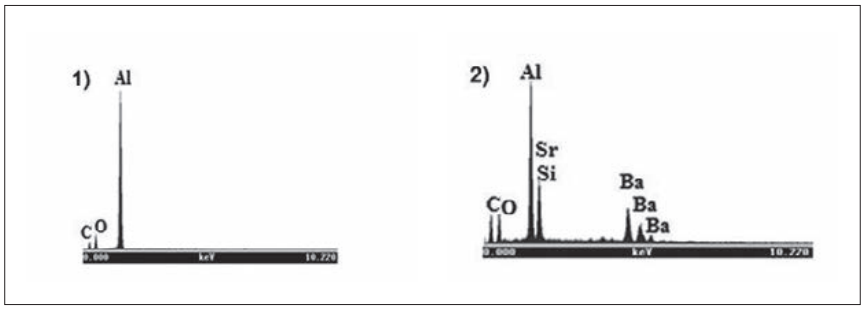

Figure 5. Typical EDS spectra obtained for the phases observed in the SEM micrographs. Key: 1) Al_2O_3 and 2) SBAS phases.

$°C^{-1}$ (37). Again, at a sintering temperature of 1500 °C and for all the studied compositions, it was observed that the degree of consolidation of the samples increased with increasing milling time. It was also observed that the SBAS crystals changed from a needle-like shape in the non-mechanically activated materials to a polyhedral morphology for the case of the samples mechanically activated for 8 h. This morphology change occurring in the SBAS crystals can be clearly noticed in Figures 3B and 4B, as well as in Figures 3D and 4D.

3.4 Hexacelsian to Celsian conversion fraction (*f*) in the sintered samples

As it can be seen in Figure 6, *f* increased with increasing sintering temperature, as well as with increasing milling time, for all the studied compositions. In the case of compositions 1 and 2, the effect of the latter factor was clearly evident at a sintering temperature of 1100 °C, while in the case of composition 3 it could be clearly noted in the temperature range of 1100-1500 °C. In all cases, a value of $f \cong 0$ was obtained at a sintering temperature of 900 °C, independently of milling time. On the other hand, composition 1 achieved a nearly constant value of *f*, which was very close to 100 %, independently of both milling time and sintering temperature, in the temperature range of 1300-1500 °C. A similar situation was also observed in the case of composition 2 milled either for 4 h or 8 h, as well as for composition 3 milled for 8 h. Thus, with decreasing nominal content of SBAS in the composites, a longer milling time was required in order to obtain a value of *f* close to 100 % in the temperature

Bol. Soc. Esp. Ceram. Vidr. Vol 53. 3, 121-132, Mayo-Junio 2014. ISSN 0366-3175. eISSN 2173-0431. doi: 10.3989/cyv.162014

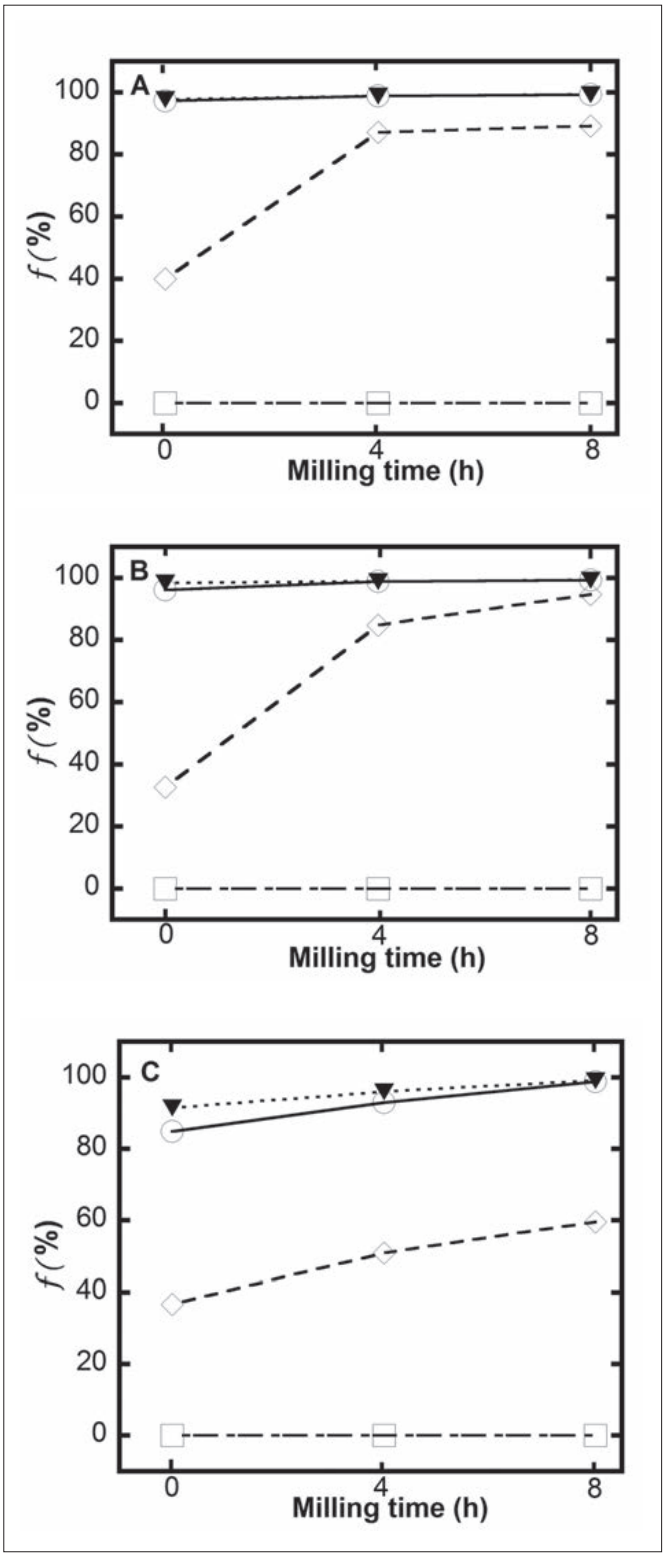

Figure 6. Hexacelsian to Celsian conversion fraction as a function of milling time for: A) composition 1, B) composition 2, and C) composition 3, sintered at 900 °C (□), 1100 °C (◇), 1300 °C (○) and 1500 °C (▼).

range of 1300-1500 °C. Once this goal was achieved, the sintering temperature made no significant difference in the value of *f*, within the mentioned temperature range. This suggests that the Hexacelsian to Celsian conversion was more difficult when the nominal content of SBAS was decreased in the composites, and that this difficulty could be overcome by mechanical activation of the corresponding precursor mixtures. Composition 1 seemed to have the strongest intrinsic tendency toward the achievement of full Hexacelsian to Celsian conversion, among the studied compositions, in such a way that compositions 2 and 3 were the most dependent on the mechanical activation of the precursor mixtures in order to achieve the same goal.

The tendency toward an easier Hexacelsian to Celsian conversion shown by composition 1 could be explained based on the combined effect of three factors: 1) this composition had the highest content of $BaCO_3$ and $SrCO_3$ among all the studied materials, and these carbonates were the components of the precursor mixtures that were the most affected by mechanical activation, which significantly increased their reactivity toward other compounds mixed with them; 2) composition 1 also had the highest proportion of fluxing agents such as $BaCO_3$ and $SrCO_3$, as well as the highest proportion of FA, and some of the impurities contained in the latter material, such as alkaline metal oxides (Na_2O and K_2O), alkaline-earth metal oxides (CaO and MgO) and iron oxides, are also powerful fluxing agents; K. H. Sandhage et al. (38,39) mentioned that the formation of Celsian from BAS glass precursors is facilitated by the presence in them of a fluxing agent or by Celsian seeding, and that the formation of a transient liquid during sintering of the materials enhances the Hexacelsian to Celsian conversion in them, which is likely due to a dissolution/reprecipitation mechanism, and 3) some of the FA impurities (Na_2O, CaO, TiO_2 and MgO), of which composition 1 also had the highest proportion, seem to have a mineralizing effect that facilitates the Hexacelsian to Celsian conversion in the materials, as suggested by D. Long-González et al. (5); the ~70 wt. % of a silicoaluminous glassy phase contained in the conditioned FA could also have contributed to the formation of the transient liquid during sintering of the materials.

The synergistic effect of the previously discussed factors with the mechanical activation of the precursor mixtures could help us to explain the seemingly contradictory results obtained in this work, with respect to those previously reported by S. Bosković et al. (17) for BAS materials synthesized from mechanically-activated reagent grade raw materials, who found that mechanical activation promoted the surface nucleation of Hexacelsian under the particular experimental conditions employed by them. As already mentioned, in this work under certain circumstances the Hexacelsian to Celsian conversion was promoted by an increased milling time, i.e, by a decreased particle size achieved in the precursor mixtures. In this sense, our results are more in line with those reported by C.M. López-Badillo et al. (24), who employed the same raw materials and milling conditions used by us for the synthesis of BAS materials.

3.5. Evaluation of relative density of the sintered materials

As it can be seen in Table II, in general the relative density of the composite materials tended to increase with increasing sintering temperature and milling time. The relative density also increased with increasing content of $BaCO_3$, $SrCO_3$ and FA, i.e. with decreasing content of Al_2O_3, in the precursor mixtures. This coincided with the conditions under which the highest values of the Hexacelsian to Celsian conversion tended to be obtained. In this way, the maximum relative

TABLE II. RELATIVE DENSITY OF THE SYNTHESIZED SBAS-Al_2O_3 COMPOSITES, AS A FUNCTION OF MILLING TIME AND SINTERING TEMPERATURE.

Composition	ρ_T (g/cm³)	Milling time (h)	Sintering temperature (°C)			
			900	1100	1300	1500
1	3.37	0	0.66	0.70	0.80	0.90
		4	0.76	0.79	0.83	0.97
		8	0.79	0.80	0.96	1.00
2	3.49	0	0.69	0.70	0.72	0.86
		4	0.71	0.78	0.80	0.89
		8	0.75	0.79	0.82	0.92
3	3.61	0	0.66	0.71	0.74	0.76
		4	0.68	0.72	0.76	0.79
		8	0.69	0.75	0.80	0.95

TABLE III. VALUES OF YOUNG'S MODULUS (GPA) OBTAINED FOR THE STUDIED COMPOSITIONS AS A FUNCTION OF MILLING TIME AND SINTERING TEMPERATURE. THE STANDARD ERROR IS GIVEN FOR ALL THE REPORTED MEASUREMENTS. KEY: E(U) = YOUNG'S MODULUS DETERMINED BY AN ULTRASONIC INSPECTION TECHNIQUE, AND E(MT) = YOUNG'S MODULUS DETERMINED BY MECHANICAL TESTING.

Composition	Milling time (h)	Sintering temperature (°C)					
		1100		1300		1500	
		E (U)	E (EM)	E (U)	E (EM)	E (U)	E (EM)
1	0	1.90 ± 7.64	---	2.63 ± 0.15	2.04 ± 0.07	10.86 ± 1.73	12.10 ± 1.75
	4	3.68 ± 4.02	3.94 ± 0.43	6.48 ± 1.00	9.09 ± 2.70	16.04 ± 0.58	18.98 ± 0.34
	8	8.23 ± 1.41	6.90 ± 0.03	12.76 ± 0.70	10.03 ± 1.20	31.45 ± 0.98	25.50 ± 2.77
2	0	4.91 ± 0.86	3.44 ± 0.31	8.11 ± 0.78	7.12 ± 0.69	17.40 ± 1.15	25.10 ± 3.66
	4	5.67 ± 1.75	4.66 ± 0.45	14.19 ± 1.00	12.91 ± 0.27	35.67 ± 3.24	32.98 ± 3.25
	8	9.09 ± 1.23	8.91 ± 0.71	18.16 ± 4.91	19.58 ± 1.32	76.48 ± 1.38	72.79 ± 5.27
3	0	6.70 ± 0.11	---	19.30 ± 0.58	11.43 ± 1.35	32.92 ± 0.71	18.33 ± 1.47
	4	8.32 ± 0.56	6.08 ± 1.03	27.0 ± 2.00	17.36 ± 1.25	43.78 ± 0..41	39.27 ± 5.91
	8	13.93 ± 2.10	10.27 ± 0.93	53.56 ± 1. 34	25.76 ± 0.80	93.07 ± 1.45	82.09 ± 2.38

density (~1) was achieved for composition 1 milled for 8 h and sintered at 1500 °C.

3.6. Evaluation of mechanical properties of the sintered materials

All the evaluated mechanical properties of the synthesized materials increased with increasing milling time, sintering temperature and Al_2O_3 content. This could be related to several factors. On the one hand, Al_2O_3 has better mechanical properties than SBAS. On the other hand, in the case of all compositions sintered at 1500 °C, which had a predominantly Celsian matrix, the polyhedral morphology shown by the grains of this phase in the samples milled for 8 h, instead of the needle-like shape shown by these grains in the non-mechanically activated samples, together with the highest degree of consolidation achieved by the former materials, could lead to a better distribution of the applied stresses between the matrix and the reinforcement phase in those materials, and this resulted in the attainment of the best mechanical properties in them.

The fact that the mechanical properties of the synthesized composites increased with increasing Al_2O_3 content, suggests that the particles of the latter phase acted as reinforcements, in such a way that the materials showed a behavior that is typical of particulate composites (29). In this kind of composite materials, the particle-matrix interaction cannot be treated at the atomic or molecular scale and thus continuous mechanics must be used for that. In most cases, the particulate phase is harder and stiffer than the matrix, and the reinforcing particles tend to restrain the movement of the matrix phase when a mechanical stress is applied to it. However, the particulate composites usually contain a great deal of coarse particles that do not block slip effectively. Thus, an effective reinforcement requires the presence of small particles evenly distributed throughout the matrix. The degree of improvement of their mechanical properties depends mainly on the strong bonding at the matrix-particle interface. Lastly, certain properties of these materials, such as density, elastic modulus, electrical conductivity and thermal conductivity, depend only on the relative amounts and related properties of the individual constituents, allowing us to use the Rule of Mixtures to accurately predict the value of those properties for a given composite composition.

These results also suggest that the mechanical properties of the composite materials synthesized in this work were more affected by the reinforcing effect of the Al_2O_3 particles than by the relatively small differences in relative density observed between our composite compositions milled for 8 h and sintered at 1500 °C, see Table II, all of which had a predominantly Celsian matrix.

3.6.1. YOUNG'S MODULUS

According to Table III, in many cases the values of the Young's modulus that were obtained by four-point flexural strength tests (E(EM)) were lower than those determined

Bol. Soc. Esp. Ceram. Vidr. Vol 53. 3, 121-132, Mayo-Junio 2014. ISSN 0366-3175. eISSN 2173-0431. doi: 10.3989/cyv.162014

TABLE IV. VALUES OF THE MODULUS OF RUPTURE (MOR, MPA) DETERMINED FOR THE STUDIED COMPOSITIONS AS A FUNCTION OF MILLING TIME AND SINTERING TEMPERATURE. THE STANDARD ERROR IS GIVEN FOR ALL THE REPORTED MEASUREMENTS.

Composition	Milling time (h)	Sintering temperature (°C)		
		1100	1300	1500
1	0	–––	11.25 ± 0.63	32.45 ± 5.21
	4	14.91 ± 1.30	68.78 ± 6.96	130.06 ± 9.95
	8	33.17 ± 6.59	95.34 ± 5.88	156.94 ± 0.06
2	0	12.80 ± 3.57	18.42 ± 3.91	32.82 ± 2.94
	4	14.12 ± 2.19	29.81 ± 1.03	146.93 ± 8.11
	8	16.46 ± 2.72	31.88 ± 8.65	168.99 ± 7.76
3	0	–––	43.74 ± 4.75	59.33 ± 2.76
	4	21.54 ± 4.07	55.38 ± 6.47	106.52 ± 1.53
	8	25.13 ± 3.03	47.47 ± 4.85	169.49 ± 8.18

TABLE V. FRACTURE TOUGHNESS (K_{IC}, MPA•$M^{1/2}$) DETERMINED FOR THE STUDIED COMPOSITIONS AS A FUNCTION OF MILLING TIME AND SINTERING TEMPERATURE. THE STANDARD ERROR IS GIVEN FOR ALL THE REPORTED MEASUREMENTS.

Composition	Milling time (h)	Sintering temperature (°C)		
		1100	1300	1500
1	0	---	0.45 ± 0.05	1.22 ±0.05
	4	0.49 ± 0.09	1.01 ± 0.05	2.42 ± 0.02
	8	0.89 ± 0.04	2.05 ± 0.06	3.46 ± 0.05
2	0	---	0.75 ± 0.02	1.22 ± 0.02
	4	0.38 ± 0.09	0.89 ± 0.01	2.78 ± 0.04
	8	0.60 ± 0.04	0.94 ± 0.07	3.19 ± 0.06
3	0	---	1.52 ± 0.04	2.08 ± 0.02
	4	0.83 ± 0.09	1.68 ± 0.03	2.26 ± 0.02
	8	0.96 ± 0.09	1.86 ± 0.02	6.17 ± 0.01

TABLE VI. VICKERS MICROHARDNESS (HV, KG/MM^2) DETERMINED FOR THE STUDIED COMPOSITIONS AS A FUNCTION OF MILLING TIME AND SINTERING TEMPERATURE. THE STANDARD ERROR IS GIVEN FOR ALL THE REPORTED MEASUREMENTS.

Composition	Milling time (h)	Sintering temperature (°C)		
		1100	1300	1500
1	0	–––	54.23 ± 0.36	303.23 ± 2.71
	4	9.59 ± 1.18	210.70 ± 3.25	540.72 ± 8.95
	8	31.57 ± 7.59	318.09 ± 12.58	576.53 ± 10.95
2	0	32.7 ± 6.14	80.99 ± 6.42	145.05 ± 1.15
	4	7.64 ± 0.04	139.92 ± 2.53	539.80 ± 11.51
	8	114.13 ± 7.76	255.46 ± 9.70	774.09 ± 12.16
3	0	12.65 ± 4.55	40.75 ± 6.15	511.39 ± 12.26
	4	19.29 ±1.58	53.48 ± 3.28	713.27 ± 4.15
	8	28.33 ± 3.40	60.43 ± 3.11	819.68 ± 6.79

by using the ultrasonic technique (E(U)), which was more pronounced in the case of compositions 2 and 3. The instances in which this was not the case could be explained based on the fact that the ultrasonic method does not take into account the distribution of defects in the materials. The maximum values were obtained for composition 3 milled for 8 h and sintered at 1500 °C, which were 93.07 ± 1.45 GPa according to the ultrasonic technique, and 82.09 ± 2.38 GPa according to the four-point flexural strength tests.

3.6.2. MODULUS OF RUPTURE (MOR)

The measured MOR values are shown in Table IV. As it can be seen, the maximum MOR value (169.49 ± 8.18 MPa) was obtained for composition 3 milled for 8 h and sintered at 1500 °C.

3.6.3. FRACTURE TOUGHNESS (K_{IC})

The values of K_{IC} obtained for the sintered materials are shown in Table V. As it can be seen, a maximum K_{IC} value of 6.17 ± 0.01 MPa•$m^{1/2}$ was obtained for composition 3 milled for 8 h and sintered at 1500 °C.

3.6.4. VICKERS MICROHARDNESS (HV)

The values determined for the Vickers microhardness (HV) are given in Table VI. In this case, a maximum HV value of 819.68 ± 6.79 Kg/mm^2 was obtained for composition 3 milled for 8 h and sintered at 1500 °C.

4. CONCLUSIONS

Mechanical activation of the precursor mixtures enhanced the solid state reactions, in such a way that these took place at lower temperatures and at faster rates, in comparison with the non-milled materials. Only SBAS (Hexacelsian and/or Celsian) and Al_2O_3 phases were formed in the materials sintered at 1300-1500°C. At this temperature range, composition 1 achieved a Hexacelsian to Celsian conversion very close to 100 %, independently of milling time. However, the other two investigated compositions required to be mechanically activated, with duration of the milling process increasing with an increased Al_2O_3 content in them, in order to attain similar Hexacelsian to Celsian conversions. It was hypothesized that due to its higher nominal SBAS content, composition 1 had the strongest intrinsic tendency to attain a full Hexacelsian to Celsian conversion, among the studied compositions. Lastly, the mechanical properties of all synthesized materials increased with increasing milling time, sintering temperature and Al_2O_3 content. Thus, the best mechanical properties were obtained for composition 3 milled for 8 h and sintered at 1500 °C, which were: Young's modulus of 93.07 ± 1.45 GPa (ultrasonic technique) and 82.09 ± 2.38 GPa (four-point flexural strength tests); MOR of 169.49 ± 8.18 MPa; K_{IC} value of 6.17 ± 0.01 MPa•$m^{1/2}$, and a HV value of 819.68 ± 6.79 Kg/mm^2.

ACKNOWLEDGEMENTS

The authors express their gratitude to CONACYT and Cinvestav-Saltillo for the financial support and experimental facilities provided for the development of this work. Many thanks are also given to the personnel of the "José López Portillo" power plant, Nava, Coahuila, México, for supplying the employed FA.

REFERENCES

1. Lee, K.N. (2000): Current status of environmental barrier coatings for Si-Based ceramics, *Surf. Coat. Technol.*, 133-134: 1-7.
2. Amritphale, S.S.; Anshul, A.; Chandra, N.; Ramakrishnan, N. (2007): Development of celsian ceramics from fly ash useful for X-ray radiation-shielding application, *J. Eur. Ceram. Soc.*, 27 (16): 4639-4647.
3. Beall, G.H. (2011): Refractory Glass Ceramics, *US Patent Application No. 20110072853*.
4. Bansal, N.P.; Hyatt, M.J.; Drummond III, C.H. (1991): Crystallization and properties of Sr-Ba aluminosilicate glass–ceramic matrices, *Ceram. Eng. Sci. Proc.*, 12 (7-8): 1222-1234.
5. Long-González, D.; López-Cuevas, J.; Gutierrez-Chavarría, C.A.; Pena, P.; Baudín, C.; Turrillas, X. (2010): Synthesis of monoclinic celsian from coal fly ash by using a one-step solid-state reaction process, *Ceram. Int.*, 36 (2): 661-672.
6. Sirazhiddinov, I.A.; Arifov, P.A.; Grebenshchikov, R.G. (1972): Isomorphism in the system $SrAl_2Si_2O_8$-$BaAl_2Si_2O_8$, *Neorgan. Mat.*, 8: 870-875.
7. Bansal, N.P. (1998): Solid state synthesis and properties of monoclinic celsian, *J. Mater. Sci.*, 33 (19): 4711-4715.
8. Lin, H.C.; Foster, W.R. (1968): Studies in the system BaO-Al_2O_3-SiO_2. I. The polymorphism of celsian, *Am. Mineral.*, 53 (1–2): 134-144.
9. Lee, K.-T.; Aswath, P.B. (2003): Role of mineralizers on the hexacelsian to celsian transformation in the barium aluminosilicate (BAS) system, *Mater. Sci. Eng.*, A 352 (1-2): 1-7.
10. Khater, G.A.; Idris, M.H. (2007): Role of TiO_2 and ZrO_2 on crystallizing phases and microstructure in Li, Ba aluminosilicate glass, *Ceram. Int.*, 33 (2): 233-238.
11. Moya Corral, J.S.; Verduch, G. (1978): The solid solution of silica in celsian, *Trans. J. Br. Ceram. Soc.*, 77 (2): 40-44.
12. Lee, K.-T.; Aswath, P.B. (2000): Synthesis of hexacelsian barium aluminosilicates by solid-state process, *J. Am. Ceram. Soc.*, 83 (12): 2907-2912.
13. Allameh, S.M.; Sandhage, K.H. (1997): Synthesis of celsian ($BaAl_2Si_2O_8$) from solid BaAl-Al_2O_3-SiO_2 precursors, I. XRD and SEM/EDX analyses of phase evolution, *J. Am. Ceram. Soc.*, 80 (12): 3109-3126.
14. Talmy, I.G.; Haught, D.A. (1991): Low temperature synthesis of high purity monoclinic celsian using topaz, *US Patent No. 4,994,419*.
15. Guillem Villar, M.C.; Guillem Bonzonis, C.; Navarro, J.A. (1983): Reactions between Kaolin and barium carbonate: influence of mineralizers. I Qualitative study, *Trans. J. Br. Ceram. Soc.*, 82 (2): 69-72.
16. Lee, K.-T.; Aswath, P.B. (2001): Enhanced production of celsian barium aluminosilicates by a three-step firing technique, *Mater. Chem. Phys.*, 71 (1): 47-52.
17. Bosković, S.; Kosanović, D.; Bahloul-Hourlier, Dj.; Thomas, P.; Kiss, S.J. (1999): Formation of celsian from mechanically activated $BaCO_3$-Al_2O_3-SiO_2 mixtures, *J. Alloys Compd.*, 290 (1-2): 230-235.
18. Semler, C.E.; Foster, W.R. (1969): Studies in the System BaO-Al_2O_3-SiO_2: IV, The System Celsian-Alumina and the Join Celsian-Mullite, *J. Am. Ceram. Soc.*, 52(12): 679-680.
19. Shukla, A. (2012): *Development of a Critically Evaluated Thermodynamic Database for the Systems Containing Alkaline-Earth Oxides*, Doctoral Dissertation, École Polytechnique de Montréal, Montréal, Canada.
20. Zhang, C.; Zhang, F.; Cao, W.S.; Chang, Y.A. (2010): Thermodynamic modeling of the Al-Si-Sr-O quaternary system, *Intermetallics*, 18(8): 1419-1427.
21. Paul, S.D. (1957): Sub-liquidus equilibria for the ternary system SrO-Al_2O_3-SiO_2, *Bull. Va. Polytech. Inst.*, 50 (11): 1-12.
22. López-Cuevas, J.; Ramos-Ramírez, M.V.; Rodríguez-Galicia, J.L. (2013): Synthesis and characterization of ceramic composites of the binary system $Ba_{0.75}Sr_{0.25}AlSi_2O_8$ - Al_2O_3. In *MRS Proceedings Vol. 1485*, Cambridge University Press, USA, pp. 107-112.
23. Medina, A.; Gamero, P.; Querol, X.; Moreno, N.; De León, B.; Almanza, M.; Vargas, G.; Izquierdo, M.; Font, O. (2010): Fly ash from a mexican mineral coal I: Mineralogical and chemical characterization, *J. Hazard. Mater.*, 181 (1-3): 82-90.
24. López-Badillo, C.M.; López-Cuevas, J.; Rodríguez-Galicia, J.L.; Pech-Canul, M.I. (2013): Synthesis and characterization of $BaAl_2Si_2O_8$ using mechanically activated precursor mixtures containing coal fly ash, *J. Eur. Ceram. Soc.*, 33 (15-16): 3287-3300.
25. López-Cuevas, J.; Long-González, D.; Gutiérrez-Chavarría, C.A. (2012): Effect of milling time on the physical and mechanical properties of celsian-mullite composites synthesized from coal fly ash. In *MRS Proceedings Vol. 1373*, Cambridge University Press, USA, pp. 43-52.
26. López-Badillo, C.M.; López-Cuevas, J.; Rodríguez-Galicia, J.L. (2007): Activación mecanoquímica de ceniza volante y $BaCO_3$ para la obtención de celsiana de bario. In *Proceedings of the XLVII Congreso Anual de la Sociedad Española de Cerámica y Vidrio*, Sociedad Española de Cerámica y Vidrio, Toledo, Spain.
27. Standard specification for coal fly ash and raw or calcined natural pozzolan for use in concrete. In *ASTM C 618-03 (2003)*, ASTM International, West Conshohocken, PA., USA.
28. Chung, F.H. (1974): Quantitative interpretation of X-ray diffraction patterns of mixtures, I. Matrix-flushing method for quantitative multicomponent analysis, *J. Appl. Crystallogr.*, 7 (6): 519-525.
29. Askeland, D.R.; Fulay, P.P., and Wright, W.J. (2010): *The Science and Engineering of Materials*, Sixth Edition, Cengage Learning Inc., USA, pp. 655-658.
30. Doghmane, M.; Hadjoub, F.; Doghmane, A.; Hadjoub, Z. (2007): Approaches for evaluating Young's and shear moduli in terms of a single SAW velocity via the SAM technique, *Mater. Lett.*, 61 (3): 813-816.
31. Standard test method for flexural strength of advanced ceramics at ambient temperature. In *ASTM C 1161-02c (2002)*, ASTM International, West Conshohocken, PA., USA.
32. Standard for Fracture Toughness Testing. In *ASTM STP601-76 (1976)*, ASTM International, West Conshohocken, PA., USA.
33. Standard test method for flexural modulus of elasticity of dimension stone. In *ASTM C 1352-96 (2002)*, ASTM International, West Conshohocken, PA., USA.
34. Barsoum, M.W. (1997): *Fundamentals of ceramics*, McGraw Hill, N.Y., USA.
35. Standard Test Method for Microindentation Hardness of Materials. In *ASTM E384-99 (2003)*, ASTM International, West Conshohocken, PA., USA.
36. Criado, J.M.; Dianez, M.J.; Morales, J. (2004): Influence of the mechanical treatment on the structure and the thermal stability of alkaline-earth carbonates, *J. Mater. Sci.*, 39(16-17): 5189-5193.
37. Brown, T.L.; García, H.J.E., and Muradás, R.M.G. (2004): *Química: la ciencia central, Vol. 7*, Prentice Hall, México.
38. Sandhage, K.H.; Allameh, S.M.; Fraser, H.L. (1995): A Novel Solid Metal-Bearing Precursor (SMP) Route to Near Net-Shaped Alkaline-Earth Aluminosilicates. In Galassi, C. (ed.), *Fourth Euro-Ceramics: Basic Science - Developments in Processing of Advanced Ceramics - I*, Gruppo Editoriale Faenza Editrice, Faenza, Italy, pp. 499-506.
39. Sandhage, K.H.; Hamish, L.F. (1995): *Synthesis of High-Temperature, Monolithic Ceramic Bodies and Ceramic-Matrix Composites by the Oxidation of Solid Metal-Bearing Precursors (SMP)*, Ohio State University, Columbus Department of Materials Science and Engineering, Columbus, Ohio, USA.

Recibido: 29/01/2014
Recibida versión corregida: 31/03/2014
Aceptado: 03/04/2014